

Flame flow tagging velocimetry with 193-nm H₂O photodissociation

Joseph A. Wehrmeyer, Lubomir A. Ribarov, Douglas A. Oguss, and Robert W. Pitz

In a new nonintrusive, instantaneous flow tagging method called hydroxyl tagging velocimetry (HTV), a molecular grid of hydroxyl (OH) radicals is written into a flame and the displaced grid is imaged at a later time to give the flame's velocity profile. Single-photon photodissociation of vibrationally excited H₂O, when a 193-nm ArF excimer laser is used, produces a tag line of superequilibrium OH and H photoproducts in a high-temperature flow field that itself may contain ambient OH. The tag line OH concentration is composed mostly of direct OH photoproducts, but OH is also indirectly produced through H photoproduct reactions with oxygen-bearing species. For lean and modestly rich flames the OH tag lifetime is of the order of 1 ms. For very rich H₂-air flames (equivalence ratio of 4.4) the lifetime drops to 200 ns. After displacement the position of the OH tag line is revealed through fluorescence caused by OH (A-X) (3 ← 0) excitation by using a 248-nm tunable KrF excimer laser. A HTV grid of multiple tag lines, providing multipoint velocity information, is experimentally demonstrated in a turbulent H₂/N₂-air diffusion flame. © 1999 Optical Society of America

OCIS codes: 300.6450, 280.7250, 280.2490, 280.2470, 280.1740.

1. Introduction

Temporally resolved, single-point velocity measurements are made routinely in turbulent flows by using hot wires, laser Doppler velocimetry, and even pressure probes with moderate-frequency response. Optically based methods have advantages over insertion devices (e.g., hot wires and pressure probes). These advantages include the minimal effect on the flow field as well as the possibility of better spatial and temporal resolution. Additionally, insertion devices cannot be used in high-temperature reacting flows. If an optically based method is to be used, it is desirable that it not require gas flow vitiation by particle seeding (which is needed by laser Doppler velocimetry and sometimes by Doppler global velocimetry¹) or by the injection of a molecular tracer species (such as iodine² or nitric oxide³). Such additives can be objectionable from an environmental and/or safety aspect, and in large-scale applications they can be prohibitively costly. Biacetyl seeding⁴ of gas flows has been used for instantaneous, multipoint velocimetry,⁵ but the phosphorescence of this nontoxic tracer is easily quenched by oxygen, preventing application to air flows. Filtered Rayleigh scattering⁶ is a laser-based technique that requires no seeding but is limited to high-speed applications only because of the bandwidth characteristics of both the lasers and the optical filters typically used.

Several techniques for measuring the velocity of time-of-flight molecular flow tagging have been developed that do not require seeding. Two-photon photodissociation of water vapor (H₂O) produces a relatively short tag line of the hydroxyl radical (OH) that can be subsequently fluoresced to profile flow velocity.^{7,8} In the Raman excitation + laser-induced electronic fluorescence (RELIEF) method, a nonlinear stimulated Raman process produces a tag line of vibrationally excited oxygen (O₂) whose enhanced fluorescence excitation strength (over ground state O₂) reveals the displacement of the tag when the flow field is subsequently irradiated by an UV laser.⁹ Another technique for molecular flow tagging that uses ambient O₂ is ozone tagging velocimetry (OTV), which involves the production of a line of ozone (O₃) with a 193-nm ArF excimer laser.¹⁰ After a time delay a second laser pulse reveals the displaced O₃ tag line position by O₃ photodissociation and subsequent fluorescence of the vibrationally excited O₂ photoproduct. Both RELIEF and OTV are problematic when applied to high-temperature reacting flows. The RELIEF signal becomes obscured by fluores-

The authors are with the Department of Mechanical Engineering, Vanderbilt University, Nashville, Tennessee 37235. The e-mail address for J. A. Wehrmeyer is wehrme@vuse.vanderbilt.edu.

Received 12 April 1999; revised manuscript received 11 August 1999.

0003-6935/99/336912-06\$15.00/0

© 1999 Optical Society of America

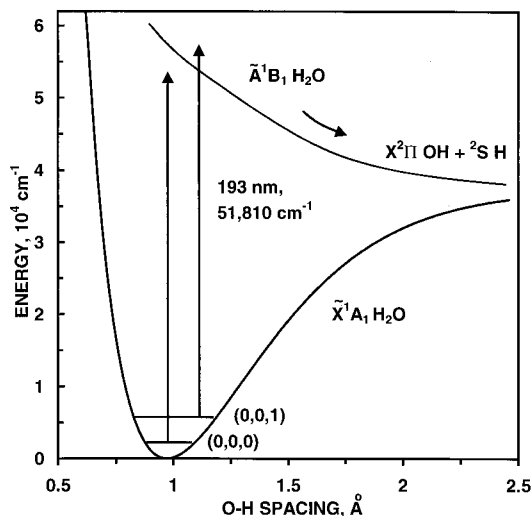


Fig. 1. H_2O energy level diagram. Ground-state data from Ref. 12; excited-state data from Ref. 13. Both curves are for the equilibrium bond angle (104.5°) and equilibrium spacing (0.97 \AA) for the second OH bond.

cence from ambient vibrationally excited O_2 , and the signal strength is reduced by H_2O quenching. For OTV at high temperature, the O_3 produced from O_2 photodissociation is quickly destroyed by thermal decomposition, reducing both the O_3 lifetime and the peak O_3 concentration.¹¹

In this paper we describe a new technique for molecular flow tagging called hydroxyl tagging velocimetry (HTV). It is amenable to high temperature reacting flow fields, and can produce relatively long tag lines by virtue of its single-photon write and read steps. When an ArF excimer laser is used, photodissociation of vibrationally excited H_2O creates a line of OH at a concentration higher than the ambient OH. The OH superequilibrium line is displaced and then irradiated with a KrF excimer laser light sheet to reveal the location of the displaced tag line by OH fluorescence. The HTV demonstration in this paper uses a single laser sheet and thus does not show out-of-plane velocity information.

2. H_2O Photodissociation and OH Photoproduct Lifetime

For H_2O vibrational motion there are three fundamental frequencies (ν_1, ν_2, ν_3) for three modes: symmetric stretch ($\nu_1 = 3651 \text{ cm}^{-1}$), bending ($\nu_2 = 1595 \text{ cm}^{-1}$), and asymmetric stretch ($\nu_3 = 3756 \text{ cm}^{-1}$). Figure 1 shows curves of the potential energy surfaces for the ground (\tilde{X}^1A_1) and first excited (\tilde{A}^1B_1) electronic states of H_2O . The \tilde{A}^1B_1 state is a repulsive state with an energy relative to the ground state of at least $53,800 \text{ cm}^{-1}$ for O–H spacings typically encompassed by ground-state H_2O . Thus the first absorption band for H_2O has a high wavelength cutoff at $\sim 185 \text{ nm}$ for low-temperature (atmospheric conditions) H_2O .¹⁴ The photon energy of 193-nm radiation ($51,813 \text{ cm}^{-1}$) is too low for absorption by ground vibrational state H_2O , but absorption by vibra-

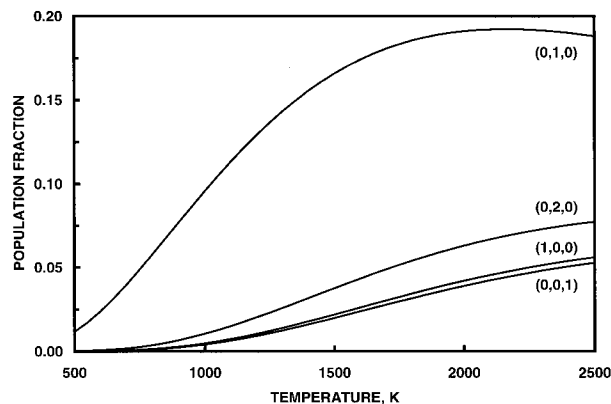


Fig. 2. H_2O equilibrium vibrational level population fractions versus temperature for first four vibrationally excited levels.

tionally excited H_2O is possible. As a simplistic example, H_2O in the $(0, 0, 1)$ state needs only $53,800 - 3756 = 50,044 \text{ cm}^{-1}$ of photon energy for appreciable absorption to occur. The 193-nm absorption cross section by the $(0, 0, 1)$ state is approximately 500 times that for ground-state H_2O , and the enhanced absorption strength of vibrationally excited H_2O has been used to study photodissociation dynamics of particular rovibrational levels through IR–UV pump–probe experiments.¹⁵ Although $(0, 1, 0)$ has little enhanced absorption compared with the ground state, the $(0, 2, 0)$, $(1, 0, 0)$, and $(0, 0, 1)$ levels all have sufficient vibrational energy to allow enhanced 193-nm absorption. In addition, these three vibrational levels have significant populations at flame temperatures: $\sim 3\%$ for each at 1500 K and $\sim 5\%$ for each at 2000 K. This is shown in Fig. 2 where equilibrium H_2O vibrational population fractions are plotted versus temperature.

As vibrationally excited H_2O is pumped by 193-nm excitation into the repulsive \tilde{A}^1B_1 state, it produces OH and H through direct fragmentation. The line of photofragments can then be convected by the flow field, and its displaced location is revealed by OH fluorescence. The KrF laser used in the present work accesses several rotational lines of the $\tilde{A}^2\Sigma^+ - \tilde{X}^2\Pi$ ($3 \leftarrow 0$) OH band that lie in the laser's output range (from 248 to 249 nm).¹⁶

The tag line created by the ArF laser consists of both OH and H photofragments superimposed on a reacting flow field containing ambient amounts of OH that can obscure detection of the tag line. In addition, the reactive OH tag molecule cannot exist for long periods in the high-temperature flow field in which it is created. To assess these issues, the SENKIN application¹⁷ is used to simulate a constant-pressure, adiabatic system that initially contains an equilibrium mixture of hot products from H_2 –air combustion along with additional amounts of OH and H photoproducts. The chemical reaction mechanism used is an abridged version of the Gas Research Institute's GRI-Mech 2.11 mechanism that retains reactions involving only noncarbon-

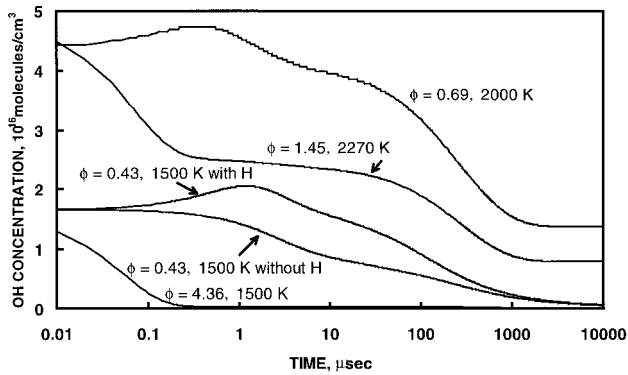


Fig. 3. OH concentration versus time for four H_2 -air postflame flows, initially including H_2O photodissociation OH and H photoproducts. The $\phi = 0.43$ flame was also modeled without the H photoproduct.

bearing species.¹⁸ The OH time histories for several initial conditions are shown in Fig. 3. Adiabatic equilibrium temperatures and equivalence ratios (ϕ) used for initial conditions are also shown in Fig. 3. The amount of H_2O photodissociated is assumed to be the total H_2O concentration multiplied by the population fraction of the (0, 0, 1) level, assuming a transition probability of 100%. The large ground-state H_2O absorption coefficient at 180 nm (Ref. 14) suggests that the 193-nm transition probability is high for the vibrationally excited levels, and experimental results show that the OH photoproduct concentration is at least an order of magnitude higher than the ambient OH.

Recently, absorption cross sections for the five lowest-lying vibrational levels have been estimated¹⁹ by using three-dimensional wave packet calculations²⁰ that employ a \tilde{X}^1A_1 ground-state potential surface²¹ fitted to experimental data and an *ab initio* \tilde{A}^1B_1 excited-state surface. At 193 nm the predicted cross sections for the vibrationally excited states, in units of 10^{-18} cm^2 , are 0.0042 ± 0.001 for (0, 1, 0), 0.0161 ± 0.003 for (0, 2, 0), 0.37 ± 0.05 for (0, 0, 1), and 1.9 ± 0.3 for (1, 0, 0). These calculations assume that the H_2O is rotationally cold ($J'' = 0$), and they predict that $\sim 98\%$ of the OH photoproduct is in the vibrational ground state. Compared with the ground-state value of $0.0008 \times 10^{-18} \text{ cm}^2$, the excited-state cross sections are greater by factors of 5 (0, 1, 0), 20 (0, 2, 0), 460 (0, 0, 1), and 2370 (1, 0, 0). The large cross sections for the (1, 0, 0) and the (0, 0, 1) states ensure almost complete photodissociation of those H_2O populations at the laser fluence levels used in the present work. Thus the assumption of only (0, 0, 1) participation, at 100% efficiency, is conservative for the OH photoproduct lifetime calculations.

Figure 3 shows that, for the two lean flames with initial adiabatic flame temperatures of 1500 and 2000 K, the OH tag line persists until ~ 1 ms when the OH concentration has almost fully decayed to its equilibrium concentration. For the 2000-K lean flame the ambient OH concentration and the

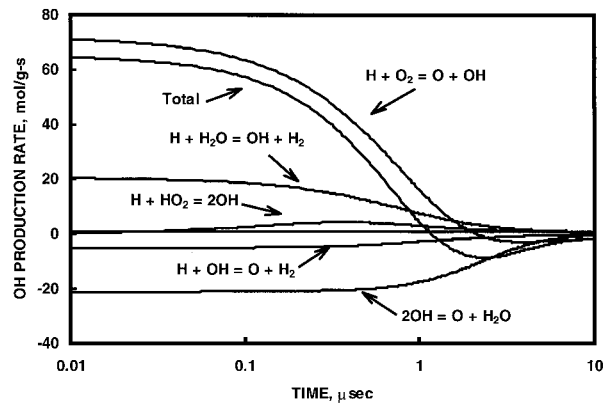


Fig. 4. Production rates for most significant OH production or destruction reactions for the $\phi = 0.43$ H_2 -air flame (from Fig. 3) with initial OH and H photoproducts.

H_2O (0, 0, 1) population fraction are both higher than for the 1500-K flame, leading to a higher signal but also to higher background noise for OH flow tag detection in the higher-temperature flame. For both of these lean flames, before the OH concentration decays to equilibrium, there is additional production of OH beyond that created directly from photodissociation. The most important OH production rates are displayed in Fig. 4 as functions of time for the $\phi = 0.43$ flame. To as high as $\sim 1 \mu\text{s}$, the reaction responsible for much of the postphotodissociation OH production is $\text{H} + \text{O}_2 \rightarrow \text{OH} + \text{O}$ and to a lesser extent the reaction $\text{H} + \text{H}_2\text{O} \rightarrow \text{OH} + \text{H}_2$. Both of these reactions consume the superequilibrium H atoms formed by H_2O photodissociation. Figure 3 shows an additional OH concentration history for the $\phi = 0.43$ flame, in which only the equilibrium H (essentially nonexistent) is present initially rather than the additional H photoproduct. For this situation there is no additional postphotodissociation production of OH and its concentration drops monotonically with time. Data for two rich flame conditions are shown in Fig. 3 with the H atom photoproduct concentration included initially. For the $\phi = 1.45$ flame the initial OH photoproduct concentration decays to approximately half of its value within 200 ns and, for the very rich ($\phi = 4.36$) flame, almost fully decays within 200 ns. The decreased OH lifetime in the rich flames, and the monotonic nature of their OH concentration histories, are due mainly to the reaction $\text{OH} + \text{H}_2 \rightarrow \text{H}_2\text{O} + \text{H}$, which removes the OH photoproduct by its reaction with excess H_2 fuel. This is shown in Fig. 5, which graphs, for the $\phi = 1.45$ flame, the production (or destruction) rate histories for the most important OH reactions. In Fig. 3 the two-tiered OH concentration history for the $\phi = 1.45$ flame is due to the fast removal of OH photoproducts by excess fuel (as shown in the above reaction) within $\sim 1 \mu\text{s}$, whereas at longer time scales this reaction ceases to be the predominant OH removal mechanism. In the $\phi = 4.3$ flame

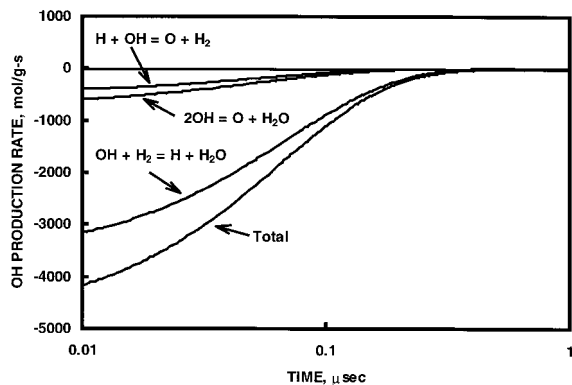


Fig. 5. Production rates for the most significant OH production or destruction reactions for the $\phi = 1.45$ H_2 -air flame (from Fig. 3) with initial OH and H photoproducts.

there is enough excess fuel to remove completely the OH photoproducts within $1 \mu s$.

3. Experimental

Two narrow-band Lambda-Physik COMPex-150T excimer lasers are used for the following hot H_2O flow tagging demonstration. Figure 6 shows a schematic of the experimental system with two grid lines. The write laser has ~ 150 mJ of ~ 193 -nm output energy with only $\sim 50\%$ arriving at the sample volume through 1 m of air. The read laser's output is ~ 400 mJ at ~ 248 nm with a tunable bandwidth of 0.001 nm and is tuned to excite the $A^2\Sigma^+ - X^2\Pi$ ($3 \leftarrow 0$) $P_1(8)$ OH transition.¹⁴ The OH fluorescence emission is imaged with a gated, intensified CCD camera coupled to an $f/4.5$ UV imaging lens. The intensifier is gated on for 100 ns only during the firing of the read pulse so that 193-nm scattering is not detected, nor is the background flame luminosity. A Schott WG-305 filter is placed in front of the camera to filter out both the 248-nm Rayleigh and Mie scattering. We created a grid of tag lines by splitting the 193-nm write laser into six beams, each focused by separate 500-mm focal-length lenses. Nine grid crossing points occur, with each crossing point providing an unambiguous location to determine displacement.

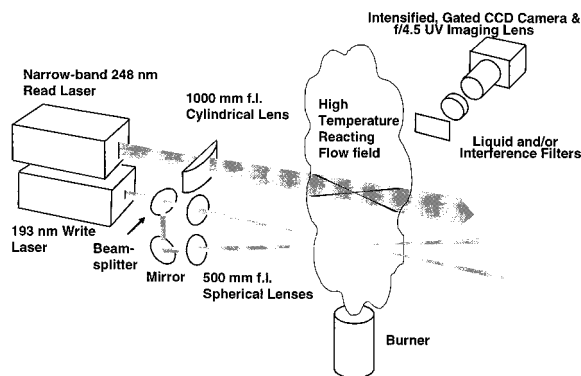


Fig. 6. Experimental system schematic showing optics needed for two tag lines only.

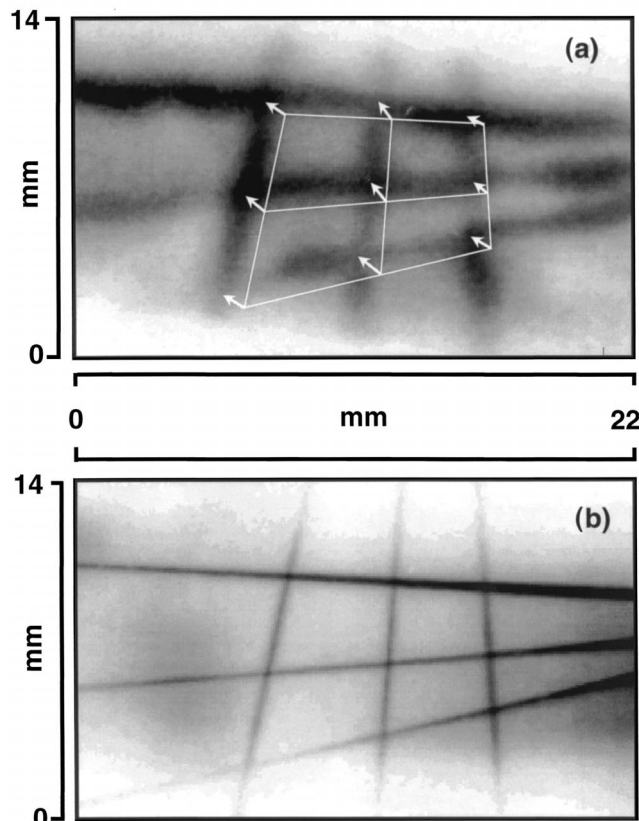


Fig. 7. Single-pulse OH fluorescence images from hot H_2O photodissociation, taken in turbulent H_2/N_2 -air diffusion flame. Write-read delays: (a) $50 \mu s$, (b) $0 \mu s$.

4. Results

The demonstration flow field is a turbulent H_2/N_2 -air diffusion flame created by a nozzle 1.8 mm in diameter issuing N_2 -diluted H_2 into quiescent air. The measured flow rates (at $0^\circ C$ STP) are ~ 40 liters/min of H_2 and 4 liters/min for N_2 . A $50\text{-}\mu s$ write-read delay is used. Figure 7(a) shows a typical instantaneous image of the displaced hot tag grid. This is for a location ~ 40 mm (22 diameters) downstream of the jet exit near the jet centerline. The flow proceeds from the figure's bottom right corner up to the upper left corner. Figure 7(b) shows another image of the hot tag grid where the write-read delay time is $0 \mu s$, thus providing the initial locations of the hot tag grid. These initial locations are indicated on Fig. 7(a) by the superimposed initial grid; displacement vectors are also shown. The length estimate for the center displacement vector is 1.1 mm, which, when divided by the $50\text{-}\mu s$ write-read delay time, gives a measured velocity of 22 m/s.

The velocity measurement uncertainty is dominated by the displacement measurement uncertainty, inasmuch as the write-read delay is known to within 4 ns, or $\sim 0.1\%$ of the $50\text{-}\mu s$ value used. The displacement measurement uncertainty depends on uncertainties in measuring the initial and final grid locations. Of these two, the final location uncertainty is higher because molecular diffusion spreads

out the tag line from its initial tightly focused size. The displaced tag-line size can be estimated by using²²

$$w = [8 \ln(2)\Delta t D + w_0^2]^{1/2},$$

where w is the tag-line width after a delay time Δt , w_0 is the initial tag-line width, and D is an appropriate diffusion coefficient. When D is estimated at $10 \text{ cm}^2/\text{s}$, the binary diffusion coefficient of OH into N_2 at 2340 K (the adiabatic flame temperature for this H_2/N_2 -air flow field), the above equation gives an expected tag-line width of $\sim 600 \text{ }\mu\text{m}$. This assumes that w_0 is $250 \text{ }\mu\text{m}$, which is typical for 500-mm focal-length lenses at 193 nm. The average w in Fig. 7(a) is significantly larger than $600 \text{ }\mu\text{m}$, being closer to 1.5 mm. This could at least be partially explained by the additional formation of OH by the H photoproduct. Before H reacts to form OH, it diffuses from the tag line at a faster rate than the heavier OH molecule. The binary diffusion coefficient for H into N_2 is ~ 4 times that for OH, and as a result the tag-line width is predicted to be about twice as great, or 1.2 mm. A rough estimate of the ability to determine the center of the diffusion-broadened displaced line is to assume that it can be measured to within one tenth of the tag line's width. Using the experimentally determined width of 1.5 mm results in an uncertainty of $150 \text{ }\mu\text{m}$, which is 14% of the displacement vector. Thus for these conditions the velocity can be estimated to within $\sim 14\%$ of its value. This uncertainty will improve going from the relatively low-velocity flow demonstrated here to high-velocity combustion flows. Thus a prime application of hot water vapor flow tagging velocimetry is to high-temperature, high-speed environments found in aer propulsion, especially in supersonic ramjets.

5. Summary and Conclusions

When a 193-nm ArF excimer laser is used, vibrationally excited H_2O is photodissociated to form OH and H photoproducts, creating a tag line of super-equilibrium OH in a high-temperature flow field that itself may contain ambient OH. The relative concentrations of the ambient and tag-line OH depends on temperature as well as the amount of H_2O present. As temperature rises the ambient OH concentration rises, but also the percentage of H_2O in vibrationally excited states increases. The tag-line OH concentration is composed mostly of direct OH photoproducts, but OH is also indirectly produced through reactions involving the H photoproduct. For lean flames the OH tag lifetime is of the order of 1 ms, whereas for rich flames the lifetime can be significantly less, with the lifetime dropping to 200 ns for very rich H_2 -air flames. The mechanism for this OH tag depletion in rich H_2 -fueled flames is the reaction $\text{OH} + \text{H}_2$ forming $\text{H}_2\text{O} + \text{H}$. After displacement we revealed the OH tag line through fluorescence caused by $\text{A } ^2\Sigma^+ - \text{X } ^2\Pi$ ($3 \leftarrow 0$) excitation by using a 248-nm tunable KrF excimer laser.

For the experimental demonstration shown in this

paper, both lasers are tunable, although it is unnecessary for the ArF laser, because the H_2O absorption band is a broad continuum with no distinct absorption lines. Also a 308-nm XeCl excimer laser could be a better choice for the read laser since stronger $\text{A } ^2\Sigma^+ - \text{X } ^2\Pi$ ($0 \leftarrow 0$) transitions can be accessed. We chose the present two lasers in an effort to develop HTV as a velocimetry method that can be performed simultaneously with OTV, which requires tunable ArF and KrF lasers. This would allow OTV and HTV to be used simultaneously to measure velocities in adjacent low- and high-temperature flows, such as are frequently encountered in combustion environments.

The experimental demonstration shown in this paper is for a reacting H_2/N_2 -air flame with a local velocity of 22 m/s, determined from a displacement vector of 1.1 mm and a write-read delay time of 50 μs . For this velocity the estimated uncertainty is $\sim 14\%$, mainly because of the spreading of the OH tag line from OH and H molecular diffusion. For faster flows requiring less delay time, diffusion should become increasingly unimportant, allowing better measurement precision. Thus a prime application of the hot water vapor flow tagging velocimetry is the high-temperature, high-speed environments found in aer propulsion, both internal and external to the engine.

Support for this research comes from NASA Glenn (NAG3-1984, Richard G. Seasholtz, technical monitor) and from a Defense University Research Instrumentation Program (DURIP) award from the Ballistic Missile Defense Organization and the Army Research Office (DAAG55-98-1-0197, David M. Mann, technical monitor). The authors thank Peter DeBarber, MetroLaser, Inc., for use of the two excimer lasers. R. W. Pitz thanks Jerry M. Seitzman, Georgia Institute of Technology, for suggesting that 193-nm H_2O photodissociation may be possible. The authors gratefully acknowledge Marc C. van Hemert and Robert van Harreveld, both of Leiden University in Leiden, The Netherlands, for calculating the H_2O excited-state absolute absorption coefficients.

References

1. R. W. Ainsworth, S. J. Thorpe, and R. J. Manners, "A new approach to flow-field measurement—a view of Doppler global velocimetry techniques," *Int. J. Heat Fluid Flow* **18**, 116–130 (1997).
2. J. C. McDaniel, B. Hiller, and R. K. Hanson, "Simultaneous multiple-point velocity measurements using laser-induced iodine fluorescence," *Opt. Lett.* **8**, 51–53 (1983).
3. G. Grünefeld, A. Gräber, A. Diekmann, S. Krüger, and P. Andresen, "Measurement system for simultaneous species densities, temperature, and velocity double-pulse measurements in turbulent hydrogen flames," *Combust. Sci. Technol.* **135**, 135–152 (1998).
4. B. Hiller, R. A. Booman, C. Hassa, and R. K. Hanson, "Velocity visualization in gas flows using laser-induced phosphorescence of biacetyl," *Rev. Sci. Instrum.* **55**, 1964–1967 (1984).

5. B. Stier and M. M. Koochesfahani, "Molecular tagging velocimetry (MTV) measurements in gas phase flows," *Exp. Fluids* **26**, 297–304 (1999).
6. J. N. Forkey, N. D. Finkelstein, W. R. Lempert, and R. B. Miles, "Demonstration and characterization of filtered Rayleigh scattering for planar velocity measurements," *AIAA J.* **34**, 442–448 (1996).
7. L. R. Boedecker, "Velocity measurements by H₂O photolysis and laser-induced fluorescence of OH," *Opt. Lett.* **14**, 473–475 (1989).
8. L. P. Goss, T. H. Chen, D. D. Trump, B. Starka, and A. S. Nejad, "Flow-tagging velocimetry using UV-photodissociation of water vapor," presented at the 29th Aerospace Sciences Meeting, Reno, Nev., 7–10 January 1991, AIAA-91-0355 (American Institute of Aeronautics and Astronautics, 1801 Alexander Bell Drive, Suite 500, Reston, Va., 1991).
9. R. B. Miles and W. R. Lempert, "Quantitative flow visualization in unseeded flows," *Annu. Rev. Fluid Mech.* **29**, 285–326 (1997).
10. R. W. Pitz, T. M. Brown, S. P. Nandula, P. A. Skaggs, P. A. DeBarber, M. S. Brown, and J. Segall, "Unseeded velocity measurement by ozone tagging velocimetry," *Opt. Lett.* **21**, 755–757 (1996).
11. L. A. Ribarov, J. A. Wehrmeyer, F. Batliwala, R. W. Pitz, and P. A. DeBarber, "Ozone tagging velocimetry using narrow-band excimer lasers," *AIAA J.* **37**, 708–714 (1999).
12. K. S. Sorbie and J. N. Murrell, "Theoretical study of the O(¹D) + H₂(¹Σ_g⁺) reactive quenching process," *Mol. Phys.* **31**, 905–920 (1976).
13. V. Staemmler and A. Palma, "CEPA calculations of potential energy surfaces for open-shell systems. IV. Photodissociation of H₂O in the \tilde{A}^1B_1 State," *Chem. Phys.* **93**, 63–69 (1985).
14. K. Watanabe and M. Zelikoff, "Absorption coefficients of water vapor in the vacuum ultraviolet," *J. Opt. Soc. Am.* **43**, 753–755 (1953).
15. D. Häusler, P. Andresen, and R. Schinke, "State to state photodissociation of H₂O in the first absorption band," *J. Chem. Phys.* **87**, 3949–3957 (1987).
16. P. Andresen, A. Bath, W. Gröger, H. W. Lülf, G. Meijer, and J. J. ter Meulen, "Laser-induced fluorescence with tunable excimer lasers as a possible method for instantaneous temperature field measurements at high pressures: checks with an atmospheric flame," *Appl. Opt.* **27**, 365–378 (1988).
17. A. E. Lutz, R. J. Kee, and J. A. Miller, "SENKIN: a Fortran program for predicting homogeneous gas-phase chemical kinetics with sensitivity analysis," Sandia Rep. SAND87–8248 (Sandia National Laboratories, Livermore, Calif., 1988).
18. J. A. Wehrmeyer, L. A. Ribarov, D. A. Oguss, F. Batliwala, R. W. Pitz, and P. A. DeBarber, "Flow tagging velocimetry for low- and high-temperature flow fields," presented at the 37th AIAA Aerospace Sciences Meeting and Exhibit, Reno, Nev., 11–14 January 1999, AIAA paper 99-0646 (American Institute of Aeronautics and Astronautics, 1801 Alexander Bell Drive, Suite 500, Reston, Va., 1999).
19. M. C. van Hemert and R. van Harrevelt, Leiden Institute of Chemistry, Gorlaeus Laboratories, P.O. Box 9502, 2300 R A Leiden, The Netherlands (personal communication, 1999).
20. G.-J. Kroes, E. F. van Dishoeck, R. A. Beärda, and M. C. van Hemert, "Photodissociation of CH₂. II. Three-dimensional wave packet calculations on dissociation through the first excited triplet state," *J. Chem. Phys.* **99**, 228–236 (1993).
21. O. Polyansky, P. Jensen, and J. Tennyson, "The potential energy surface of H₂O," *J. Chem. Phys.* **105**, 6490–6497 (1996).
22. R. Miles, W. Lempert, and B. Zhang, "Turbulent structure measurements by RELIEF flow tagging," *Fluid Dyn. Res.* **8**, No. 1, 9–17 (1991).